

Original Article

Combining "waste utilization" and "tissue to tissue" strategies to accelerate vascularization for bone repair



Zexi Li^{a,1}, Huan Wang^{b,1}, Kexin Li^b, Weishan Wang^c, Jinjin Ma^b, Zhao Liu^{b,d}, Bin Li^b, Jiaying Li^{b,**}, Fengxuan Han^{b,***}, Can Xiao^{a,*}

^a Department of Stomatology, The First Affiliated Hospital of Soochow University, Soochow University, Suzhou, Jiangsu, China

^b Medical 3D Printing Center, Orthopedic Institute, Department of Orthopedic Surgery, The First Affiliated Hospital, School of Biology and Basic Medical Sciences, Suzhou Medical College, Soochow University, Suzhou, Jiangsu, China

^c Department of Orthopaedic Surgery, The First Affiliated Hospital, Shihezi University School of Medicine, Shihezi, Xinjiang, China

^d National University of Singapore Suzhou Research Institute, Suzhou, People's Republic of China

ARTICLE INFO

Keywords:

Bone repair
Hydrogels
Microvascular fragments
Osteogenesis
Vascularization

ABSTRACT

Background: A pivotal determinant for the success of tissue regeneration lies in the establishment of sufficient vasculature. Utilizing autologous tissue grafts from donors offers the dual advantage of mitigating the risk of disease transmission and circumventing the necessity for post-transplant immunosuppression, rendering it an exemplary vascularization strategy. Among the various potential autologous donors, adipose tissue emerges as a particularly auspicious source, being both widely available and compositionally rich. Notably, adipose-derived microvascular fragments (ad-MVFs) are a promising candidate for vascularization. ad-MVFs can be isolated from adipose tissue in a short period of time and show high vascularized capacity. In this study, we extracted ad-MVFs from adipose tissue and utilized their strong angiogenic ability to accelerate bone repair by promoting vascularization.

Methods: ad-MVFs were extracted from the rat epididymis using enzymatic hydrolysis. To preserve the integrity of the blood vessels, gelatin methacryloyl (GelMA) hydrogel was chosen as the carrier for ad-MVFs in three-dimensional (3D) culture. The ad-MVFs were cultured directly on the well plates for two-dimensional (2D) culture as a control. The morphology of ad-MVFs was observed under both 2D and 3D cultures, and the release levels of vascular endothelial growth factor (VEGF) and bone morphogenetic protein 2 (BMP-2) were assessed under both culture conditions. In vitro studies investigated the impact of ad-MVFs/GelMA hydrogel on the toxicity, osteoblastic activity, and mineralization of rat bone marrow mesenchymal stem cells (rBMSCs), along with the examination of osteogenic gene and protein expression. In vivo experiments involved implanting the ad-MVFs/GelMA hydrogel into critical-size skull defects in rats, and its osteogenic ability was evaluated through radiographic and histological methods.

Results: ad-MVFs were successfully isolated from rat adipose tissue. When cultured under 2D conditions, ad-MVFs exhibited a gradual disintegration and loss of their original vascular morphology. Compared with 2D culture, ad-MVFs can not only maintain the original vascular morphology, but also connect into a network in hydrogel under 3D culture condition. Moreover, the release levels of VEGF and BMP-2 were significantly higher than those in 2D culture. Moreover, the ad-MVFs/GelMA hydrogel exhibited superior osteoinductive activity. After implanting into the skull defect of rats, the ad-MVFs/GelMA hydrogel showed obvious effects for angiogenesis and osteogenesis.

The translational potential of this article: The utilization of autologous adipose tissue as a donor presents a more direct route toward clinical translation. Anticipated future clinical applications envision the transformation of discarded adipose tissue into a valuable resource for personalized tissue repair, thereby realizing a paradigm shift in the utilization of this abundant biological material.

* Corresponding author. Department of Stomatology, The First Affiliated Hospital of Soochow University, Pinghai Rd 899, Suzhou, Jiangsu 215000, China.

** Corresponding author. Orthopedic Institute, Soochow University (North Campus), Ganjiang Rd 178, Suzhou, Jiangsu 215000, China.

*** Corresponding author. Orthopedic Institute, Soochow University (North Campus), Ganjiang Rd 178, Suzhou, Jiangsu 215000, PRChina.

E-mail addresses: lijaying@suda.edu.cn (J. Li), fxhan@suda.edu.cn (F. Han), xiaocan_0511@163.com (C. Xiao).

¹ Equal contribution as the first author

1. Introduction

The pivotal determinant for successful tissue regeneration is the establishment of adequate vascularization. The inception of novel blood vessels plays a pivotal role in fostering tissue regeneration, ensuring optimal oxygenation, and facilitating material exchange for cells within the implanted tissue [1]. Consequently, the last few decades have witnessed the introduction of myriad vascularization strategies within the realms of tissue engineering and regenerative medicine [2,3]. While prior investigations predominantly focused on approaches such as the addition of growth factors, prefabricated vascular networks, and vascular transplantation, these methodologies have grappled with issues of low efficiency and security during practical implementation [4]. Addressing these challenges necessitates an exploration of the autologous tissue vascularization strategy, which mitigates the risk of disease transmission and obviates the need for post-implantation immunosuppression. Adipose tissue emerges as a particularly promising source of autologous donors for vascularization, being widely available, frequently discarded, and exhibiting a low donor site incidence [5]. Beyond its conventional role as a lipid repository, research has unveiled adipose tissue's rich composition, encompassing fibroblasts, vascular cells, immune cells, endothelial cells, and mesenchymal stem cells [6].

A noteworthy advancement in adipose tissue-derived vascularization is the isolation of adipose tissue-derived microvascular fragments (ad-MVFs), demonstrating substantial promise as vascularization units. Endothelial cell-combined scaffolds have been reported can improve the revascularization of tissue grafts [7]. However, it may take more than a week for these cells to reassemble into new microvessels [8]. Compared to the scaffold-containing cells, the ad-MVFs show unique advantages for vascularization [9]. ad-MVFs can be enzymatically isolated from adipose tissue, obtaining natural vessel segments with an average length of 50–150 μm from arteriolar, capillary, and venular [10]. Retaining both vessel morphology and function, ad-MVFs exhibit the capacity to swiftly reassemble into new microvascular networks [11]. Reports indicate that ad-MVFs establish interconnections with blood vessels at the injury site within 3–6 days post-implantation, facilitating early onset blood perfusion within the implants [12]. As a plentiful source of multipotent mesenchymal stromal cells within their physiological niche, ad-MVFs emerge as promising candidates for generating vascularized tissue-specific substitutes [13]. Their diverse composition includes various stem cells, progenitor cells, and lymphatic vessel fragments [14], imparting an immunomodulatory effect that enhances immune acceptance of implanted scaffolds [15,16]. Applications of ad-MVFs in revascularizing diverse tissues, such as epicardial plaques [17], islet structures [18], dermal substitutes [19,20], random pattern flaps [21], and dental pulp [22], underscore their potential for effective vascularization compared to endothelial cell-combined scaffolds. Notably, numerous studies underscore the pivotal role of vascularization in bone repair processes [23]. Beyond facilitating mesenchymal stem cell migration, vascularization supplies oxygen and nutrients to metabolically active bone tissue while clearing waste products [1]. In the aftermath of bone injury, blood vessels sustain damage, leading to hematoma formation, subsequent migration of inflammatory cells to the injury site, and regulation of osteoblastic and osteoclastic progenitor cell migration by vascular endothelial cells [24,25]. New blood vessel growth is integral to the formation of a soft callus comprising fibroblasts and chondrocytes, transitioning into a calcified callus through ossification. Further mineralization and remodeling processes culminate in effective bone repair [26]. Considering these findings, the application of ad-MVF in bone defects emerges as a promising strategy for enhancing bone healing.

However, cultivating ad-MVFs in isolation for an extended duration poses significant challenges due to their diminutive size and inherent susceptibility to disintegration. Consequently, a scaffold is imperative, providing a stable milieu to preserve vascular morphology and facilitate the growth of new blood vessels. In comparison to two-dimensional (2D)

conditions, the three-dimensional (3D) culture microenvironment, facilitated by scaffolds, aptly recapitulates the native extracellular matrix, thereby fostering optimal conditions for cellular proliferation [27]. This technology, as substantiated in existing literature, holds substantial promise, offering a biomimetic microenvironment endowed with physical and biological properties conducive to microvessel growth within scaffolds [28,29]. For the construction of an optimal 3D culture microenvironment, hydrogel emerges as a judicious choice owing to its elevated water content and intricate three-dimensional network structure. Van den Bulcke et al. successfully synthesized MA-modified gelatin hydrogels (Gelatin methacryloyl, GelMA) by substituting the amino group on Gel's side chain with methacrylic anhydride (MA). It is currently a commonly used hydrogel for 3D cell culture and tissue engineering platforms. GelMA initiates atom group polymerization by ultraviolet (UV) irradiation in the presence of a water-soluble photoinitiator [30]. Characterized by its low antigenicity and stability at physiological temperature, GelMA provides an aqueous environment for the cells and supports their adhesion, growth, and proliferation, as well as promotes in-scaffold nutrient and waste of effective exchange [31]. Therefore, GelMA has been widely used in cell culture and bone tissue engineering [32], demonstrating that it helps to cultivate a favorable three-dimensional microenvironment for the growth of ad-MVFs.

In this study, ad-MVFs were encapsulated into GelMA to create ad-MVFs/GelMA hydrogels, combining "waste utilization" and "tissue-to-tissue" strategies to expedite vascularization for bone repair (Scheme 1). The ad-MVFs could grow in GelMA hydrogel, and the formation of network structure, secretion of growth factors such as BMP-2 and VEGF, and expression of CD31 will be investigated. The impact of ad-MVFs/GelMA hydrogels on the osteogenic differentiation of rBMSCs will be assessed, and the bone repair efficacy of ad-MVF/GelMA will be evaluated in a rat critical-sized skull defects.

2. Materials and methods

2.1. Isolation of the ad-MVFs

All procedures involving animals adhered to the National Institutes of Health Guidelines for the care and use of experimental animals and received approval from the animal ethics committee of Soochow University (SUDA20220711A05). The ad-MVFs were isolated from epididymal adipose tissue of Sprague Dawley (SD) male rats (weighing 350 g–400 g) by limited type I collagenase digestion (5 mg/mL, Yeasen, Shanghai, China). The samples were incubated at 37 °C for 15 min under vigorous shaking conditions. Subsequently, the suspension was centrifuged at 800 rpm for 5 min, and the supernatant was discarded. The fat cells were removed by filtration. The vascular fragments were resuspended in high glucose medium with 10 % (v/v) fetal bovine serum (FBS, Euroclone, Milan, Italy) and maintained in the humidified incubator at 37 °C with 5 % CO₂. To assess the characteristics of ad-MVFs, freshly isolated ad-MVFs were observed by an optical microscope (Carl Zeiss Inc, Thornwood, NY, USA). The ad-MVF were subjected to cryo-sectioning, and subsequently, incubated with a primary antibody (rabbit anti-CD31, 1:100, Abcam, Cambridge, UK) overnight at room temperature. This was succeeded by exposure to the corresponding IgG Alexa 594 secondary antibody (goat anti-rabbit, 1:200, Beo Tianmei, Shanghai, China) for a duration of 1 h at room temperature. Nuclear staining was conducted using DAPI 33342 (2 mg/mL, C, and the resultant images were captured using a fluorescence microscope (Carl Zeiss Inc, Thornwood, NY, USA). The diameter and length of ad-MVFs were measured using Image J software (NIH Image, Bethesda, MD, USA).

2.2. Preparation of the ad-MVFs/GelMA hydrogels

ad-MVFs/GelMA hydrogels were prepared by adding ad-MVFs into a 10 % w/v GelMA solution (with 0.25 % w/v photoinitiator) and subsequently crosslinked with blue light (405 nm wavelength) for 1 min.

2.3. Physicochemical properties of composite hydrogels

Mechanical test: The mechanical properties of cylindrical hydrogels (diameter: 4.5 mm; height: 5 mm) were assessed at a constant speed of 2 mm/min using a universal mechanical testing system (Shanghai Hengyi Precision Instrument Co., Ltd., Shanghai, China).

Degradation and swelling test: The hydrogels were submerged in a phosphate-buffered saline (PBS) solution. After 24 h, the weight of both GelMA and ad-MVFs/GelMA composite hydrogels was measured. The weight of the hydrogel post-dehydration was denoted as W_D , while the weight after reaching swelling equilibrium was labeled as W_S . The swelling rate of GelMA and ad-MVFs/GelMA was computed using the following formula:

$$\text{Swelling rate (\%)} = W_S/W_D \times 100\%$$

Subsequently, the hydrogels were immersed in PBS solution, with the initial weight of the hydrogel recorded as W_I and the final weight as W_F . The remaining mass of GelMA and ad-MVFs/GelMA was monitored over intervals of 1, 3, 5, 7, 9, 14, 21, 28, and 35 days.

$$\text{Remaining mass (\%)} = W_F/W_I \times 100\%$$

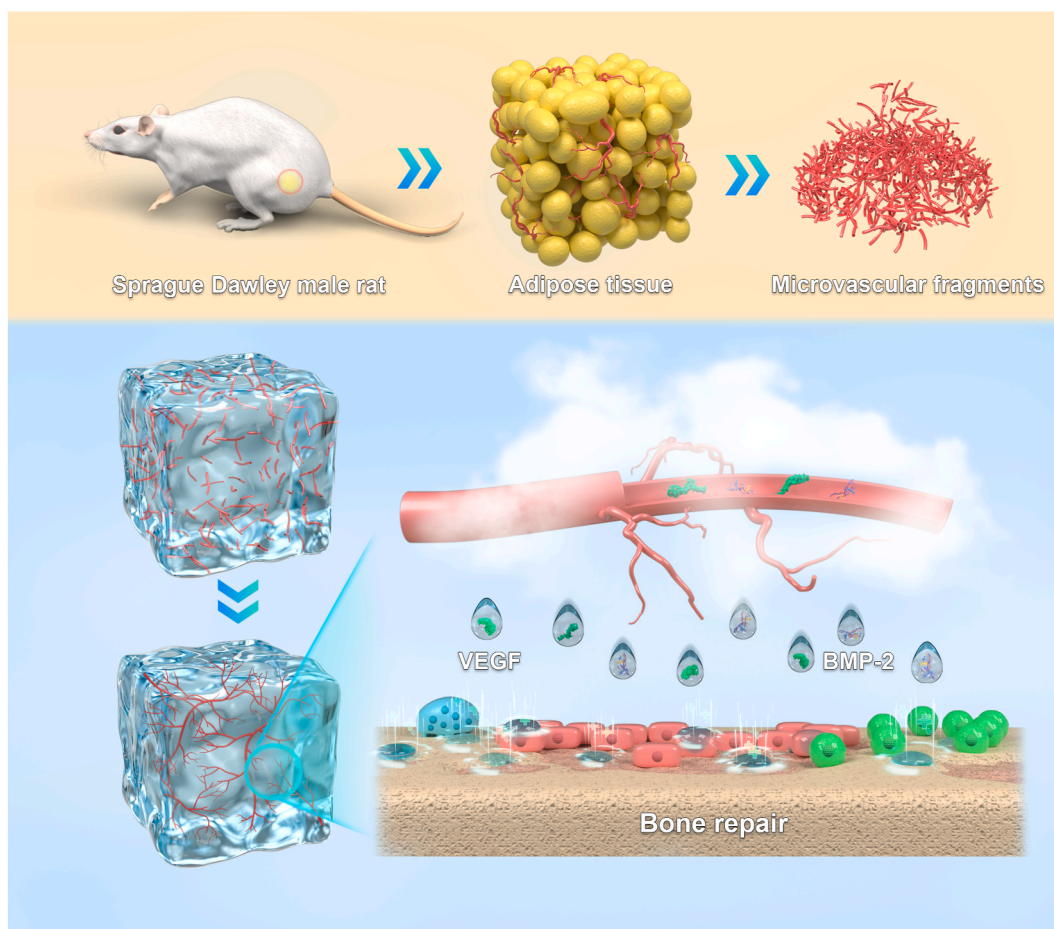
These standardized methodologies ensured accurate evaluation of the hydrogel's physicochemical characteristics, essential for comprehensively understanding their properties and potential applications.

2.4. Viability and growth of the ad-MVFs under 2D and 3D culture conditions

Under 2D culture condition, ad-MVFs were directly cultured in tissue culture plates with high glucose medium containing 10 % FBS. For 3D culture condition, ad-MVFs were added into 10 % w/v GelMA hydrogel. ad-MVFs were cultured in 3D and 2D conditions for 1, 3, 5, 7, 14, 21, 28, and 35 days, respectively. Subsequently, ad-MVFs/GelMA (3D) and ad-MVFs (2D) were fixed in 4 % paraformaldehyde for 30 min, permeabilized with 0.3 % Triton X-100 (Beyotime, Shanghai, China) for 20 min at room temperature, and blocked with immunofluorescence blocking solution (Beyotime, Shanghai, China) for 1 h. After incubation with primary antibody (rabbit anti-CD31, 1:100, Abcam, Cambridge, UK) at 4 °C overnight, the appropriate IgG Alexa 488 secondary antibody (goat anti-rabbit, 1:200, Beyotime, Shanghai, China) was applied for 1 h at room temperature. Nuclear staining was done with DAPI 33342 (2 mg/mL, Sigma-Aldrich, Munich, Germany), and images were acquired using a laser scanning confocal microscope (Zeiss LSM710/780, Oberkochen, Germany).

2.5. Measurement of VEGF and BMP-2 secreted by MVFs under 2D and 3D culture conditions

The amount of BMP-2 and VEGF released from ad-MVFs/GelMA (3D) and ad-MVFs (2D) was measured using ELISA kits (VEGF, Beyotime, Shanghai, China; BMP-2, Sangon Biotech, Shanghai, China). The culture medium of ad-MVFs/GelMA (3D) and ad-MVFs (2D) were collected on 1,



Scheme 1. The diagram of ad-MVFs isolation and experimental study design. The ad-MVFs were isolated by enzymatic digestion of the epididymal fat pads of donor rats. After removing the fat supernatant, ad-MVFs were enriched up to pellet size and mixed with GelMA. ad-MVFs rapidly form blood vascular network due to the suitable three-dimensional microenvironment provided by GelMA hydrogels. The new blood vessels are just like clouds, and VEGF and BMP-2 continuously fall from the clouds like rainwater, watering BMSCs in bone injured area and promoting bone repair.

3, 5, 7, 14, 21, 28, and 35 days, respectively. Afterward, 100 μ L supernatant from each well was analyzed by commercial ELISA kits.

2.6. Cell morphology and viability of BMSCs co-cultured with the composite hydrogel

According to the previous method [33,34], rBMSCs were extracted from the femur of rats. As a control group, rBMSCs were seeded in tissue culture plates. After 48 h of incubation, 4 % paraformaldehyde was first added to the sample to fix the cells. Then Triton X-100 was added for perforation, followed by the addition of immunofluorescence blocking solution. After that, TRITC-phalloidin was used for F-actin staining, and DAPI was used for nuclear staining.

Scanning electron microscope (SEM) was used to further observe the spreading of rBMSCs on hydrogels. The rBMSCs were seeded on different hydrogels and incubated for 48 h. The samples were fixed with 4% paraformaldehyde and dehydrated. Finally, the cell morphology was observed by SEM after drying at the critical point.

The viability of rBMSCs on hydrogels was assessed using a live dead cell staining kit (Invitrogen, Carlsbad, CA, USA). Images were acquired by a fluorescence microscope (Carl Zeiss Inc, Thornwood, NY, USA). The proliferation of rBMSCs cultured on hydrogels was determined by Cell Counting Kit-8 (CCK-8) assay (Dojin Laboratories, Kumamoto, Japan). On 1, 3, and 5 days of cell culture, CCK-8 reagents were added and incubated for 2 h. Finally, the absorbance at 450 nm was measured by BioTek Instruments (Vermont, USA).

2.7. Alkaline phosphatase (ALP) and Alizarin red staining (ARS)

rBMSCs were seeded on a six-well plate (2×10^5 cells/well), and divided into four groups: Group 1: rBMSCs were cultured with α -MEM medium (Ctrl group); Group 2: rBMSCs were cultured with osteogenic differentiation medium comprising 10 mM β -glycerophosphate, 10 nM dexamethasone, and L-ascorbic acid 2-phosphate (50 μ g/ml; Sigma–Aldrich, USA). (Induced group); Group 3: GelMA were placed in trans-well plate chambers for stratified culture with rBMSCs (GelMA group); Group 4: ad-MVFs/GelMA were placed in trans-well plate chambers for stratified culture with rBMSCs (ad-MVFs/GelMA group). The medium was changed every 2–3 days.

To detect ALP activity, rBMSCs were fixed in paraformaldehyde and stained using an ALP activity assay kit (Beyotime, Shanghai, China) after 7 days of culture. After 21 days of culture, staining was done with 0.1 % Alizarin red staining solution (Solarbio, Beijing, China). Images of red-stained calcium nodules were taken using an inverted microscope, and 5 % perchloric acid was added after the photographs were taken. Absorbance was measured at 420 nm using a microplate reader.

2.8. In vitro osteoclastic differentiation of bone marrow-derived macrophages (BMMs)

BMMs were isolated from 4-week-old mice and cultured for 24 h. Subsequently, the supernatant containing bone marrow cells was collected, centrifuged, and cultured in α -MEM supplemented with 10 % FBS, 1 % penicillin/streptomycin, and 10 ng/mL macrophage colony-stimulating factor (M-CSF) (R&D Systems, America) for 3 days. Following this, the culture medium was replaced with osteoclastic differentiation medium composed of α -MEM, 10 % fetal bovine serum, 1 % penicillin/streptomycin, 20 ng/mL M-CSF, and 50 ng/mL receptor activator of nuclear factor κ B ligand (RANKL) (R&D Systems, America).

Tartrate-resistant acid phosphatase (TRAP) staining: Osteoclastic differentiation was evaluated using TRAP staining. BMMs were seeded into the lower chamber of a 24-well transwell at a density of 1×10^4 cells per well, with various hydrogels added to the upper chamber. After 7 days of induction, the cells were stained using a TRAP staining kit (Sigma–Aldrich, Munich, Germany) following the manufacturer's instructions.

2.9. Tube formation assay

Human umbilical vein endothelial cells (HUVECs) were seeded on the surface of growth factor-reduced Matrigel at a density of 1.8×10^4 cells per well in the lower chamber of a 24-well transwell. Various hydrogels were introduced into the upper chamber. After 6 h, the morphology of HUVECs was examined using an inverted microscope, and the average parameters of tube formation across 6 randomly selected fields were quantified using ImageJ software.

2.10. Quantitative polymerase chain reaction (qPCR) detection

rBMSCs were cultured in the lower layer of 6-well trans-well plate (1×10^5 cells/well). Hydrogels (ad-MVFs/GelMA, GelMA) were placed in the trans-well chambers. On the 7th and 14th day after osteogenic induction, RNA from rBMSCs was extracted using TRIZOL reagent (Invitrogen, California, USA). The purity and concentration of RNA was measured by NanoDrop 2000 spectrophotometers (Thermo Fisher Scientific, MA, USA). RNA was reverse transcribed to cDNA using RT Master Mix (ABM, Canada). The expression of the osteogenesis-related target genes (*Alpl*, *Spp1*, *Runx2*, *Col1a1* and *Bglap*) was performed by qPCR. The primer sequences are listed in Table 1.

2.11. Western blot analysis

Total cellular protein was extracted using RIPA lysis buffer (Beyotime, Shanghai, China), resolved on 10 % SDS-PAGE gels, transferred to nitrocellulose membranes (Beyotime, Shanghai, China), and blocked in non-fat milk. Membranes were incubated with primary antibodies (rabbit anti-COL I, 1:1000, Abcam, Cambridge, UK; rabbit anti-RUNX2, 1:500 ABclonal, Boston, MA, USA; rabbit anti-OPN, 1:1000, ABclonal, Boston, MA, USA; rabbit anti-OCN, 1:1000, ABclonal, Boston, MA, USA; β -actin, 1:1000, Abcam, Cambridge, UK) in antibody dilution buffer (Beyotime, Shanghai, China). The membranes were incubated with the horseradish peroxidase-conjugated secondary antibody (goat anti-rabbit, 1:1000, Beyotime, Shanghai, China) at room temperature for 1 h. Proteins were detected by autoradiography (Bio-Rad, Hercules, CA, USA), and grayscale values were quantified with Image J software.

2.12. Animal study

In this phase of the investigation, male Sprague Dawley (SD) rats at 8 weeks of age were categorized into three groups: the Control (Ctrl) group, the GelMA group, and the ad-MVFs/GelMA group. The animals underwent intraperitoneal injection of sodium pentobarbital for anesthesia, followed by shaving and disinfection. A sagittal incision of approximately 1.5 cm was made on the cranial roof, exposing the bone surface. A full-thickness circular defect, 5 mm in diameter, was created at the center of bilateral cranial parietal bones using a trephine. Subsequently, ad-MVFs/GelMA and GelMA hydrogels were injected into the cranial defects, while the Ctrl group received an injection of phosphate buffer solution.

Table 1
PCR primer sequences.

Target gene	Forward primer sequence (5'-3')	Reverse primer sequence (5'-3')
<i>Alpl</i>	TATGTCTGGAACCGCACTGAAC	CACTAGCAAGAAGAAGCCTTTGG
<i>Spp1</i>	GCGGTTCACTTTGAGGACAC	TATGAGCGGGGATAGTCTTT
<i>Runx2</i>	ATCCAGCCACCTTCACCTACACC	GGGACCATTGGGAAGTATAGG
<i>Col1a1</i>	CAGGCTGGTGTGATGGGATT	CCAAGTCTCCAGGAACACC
<i>Bglap</i>	AACGGTGGTCCATAGATGC	AGGACCCTCTCTCTGCTCAC
<i>Gapdh</i>	GGTTGTCTCTCGCACTTCA	TGTCCAGGGTTTCTTACTCC

2.13. Micro-CT analysis

Following anesthesia induction with sodium pentobarbital, rat hearts were perfused with PBS and 4 % paraformaldehyde. The skulls were then carefully excised with scissors and fixed in 10 % formalin. After 24 h, the specimens underwent triple washing with phosphate buffer solution. Micro-computed tomography (Micro-CT) scans were conducted using SkyScan (Aartselaar, Belgium) at settings of 65 kV, 1 mm A1 filter, and 385 mA. The Skyscan NRecon program facilitated 3D reconstruction and analysis of the sample data. Additionally, the quantification of newly formed bone mass was performed.

2.14. Histology analysis

Skulls were initially fixed in formalin for 24 h, followed by immersion in 10 % EDTA decalcification solution (Sangon Biotech, Shanghai, China). After a 30-day decalcification process, specimens were dehydrated in an ethanol gradient. Femoral specimens were dehydrated in *n*-butanol overnight and then embedded in paraffin. Using a Leica paraffin microtome (Leica, Wetzlar, Germany), samples were sectioned at a thickness of 6 μ m. Hematoxylin and eosin (H&E) and Masson staining were applied to visualize new bone formation, while CD31 immunofluorescence (Abcam, Cambridge, UK) was utilized to assess vascular reconstruction. CD31 positive areas were quantified with ImageJ software.

2.15. Statistical analysis

Quantitative data are expressed as mean \pm standard deviation. Statistical analyses were conducted using Prism 8 (GraphPad Software, Inc). Significance between experimental groups was assessed via one-way analysis of variance (ANOVA), followed by Tukey's multiple comparisons. A probability value (*p*) less than 0.05 was considered statistically significant.

3. Results

3.1. Characterizations of the ad-MVFs

ad-MVFs were meticulously isolated from the epididymal adipose tissue of Sprague Dawley (SD) male rats (body weight: 350 g–400 g) through enzymatic digestion, as depicted in Fig. 1A. Immunofluorescence analysis of the extracted microvessel fragments exhibited conspicuous CD31 expression (Fig. 1B). Approximately 6000 ad-MVFs could be extracted from one side of the epididymal region, featuring diameters ranging from a few microns to tens of microns, with a prevalent range between 10 and 20 μ m (Fig. 1C). Moreover, the length of isolated ad-MVFs exceeded 400 μ m, primarily falling within the range of 100–200 μ m (Fig. 1D).

3.2. Characterization of composite hydrogels

The mechanical test results revealed that the compression modulus of the ad-MVFs/GelMA hydrogel was lower compared to that of the GelMA hydrogel, attributable to the inclusion of ad-MVFs (Fig. S1, Supporting Information). This reduction can be attributed to the disruption of the GelMA hydrogel's microstructure following the addition of ad-MVFs. Despite this decrease, the composite hydrogels maintained adequate mechanical properties, ensuring stability in shape. Degradation test further demonstrated that the degradation rate of ad-MVFs/GelMA hydrogels surpassed that of GelMA hydrogels (Fig. S2, Supporting Information). Additionally, swelling test indicated a higher swelling capacity for ad-MVFs/GelMA hydrogels compared to GelMA hydrogels (Fig. S2, Supporting Information). This may be attributed to the insufficient cross-linking of hydrogel molecular chains induced by ad-MVFs, facilitating easier penetration of water molecules into the

hydrogel matrix. Consequently, this enhances the hydrogel's water-absorbing capacity and overall swelling degree.

3.3. The growth of ad-MVFs under 2D and 3D culture conditions

To assess the viability and growth of ad-MVFs, isolated from the adipose tissue of the epididymal regions, under different conditions, cultures were conducted in both 2D and 3D settings. In the 2D culture condition, ad-MVFs retained their vascular morphology on the first day post-extraction but displayed disintegration on the second day, eventually regrowing on the plate (Fig. 1E). Conversely, 3D culture within GelMA hydrogel provided a conducive microenvironment for ad-MVFs, facilitating their assembly into a vascular network (Fig. 1E). Under 3D culture conditions, ad-MVFs exhibited proliferative behavior, forming a complex capillary network by day 7. Additionally, some cells within ad-MVFs displayed altered morphology, generating membrane protrusions like filopodia and forming new sprouts from tip cells. Notably, ad-MVFs supported the generation of new lateral branches in the microvessels. By day 35, a well-formed capillary network had emerged under 3D culture conditions.

3.4. Secretion of VEGF and BMP-2 by ad-MVFs under 2D and 3D culture conditions

The secretion of VEGF and BMP-2 from ad-MVFs was examined under both 2D and 3D culture conditions. Results indicated an increase in both VEGF and BMP-2 secretion over time. In the early stages, VEGF release from ad-MVFs/GelMA (3D) mirrored that of ad-MVFs (2D). However, after 7 days, VEGF secretion in the 3D setting surpassed that in the 2D condition. BMP-2 secretion from ad-MVFs/GelMA was slightly lower than ad-MVFs at 2D during the initial 2 weeks but exhibited higher levels in the later period under 3D culture conditions (Fig. 1F and G).

3.5. Morphology and proliferation of rBMSCs on the surface of the ad-MVFs/GelMA hydrogels

Cytocompatibility of ad-MVFs/GelMA hydrogels was assessed by seeding rBMSCs on the hydrogel surface. Cytoskeleton staining revealed robust cell adhesion and spreading on both GelMA and ad-MVFs/GelMA hydrogels after 48 h, indicating excellent biocompatibility. SEM images further confirmed successful cell growth on the hydrogel surfaces (Fig. 2A and B). Live/dead staining and CCK-8 assay results demonstrated negligible cytotoxicity and consistent proliferation of rBMSCs across all groups during the culture process, confirming the favorable biocompatibility of ad-MVFs/GelMA hydrogels (Fig. 2C and D).

3.6. In vitro osteogenic differentiation of rBMSCs co-cultured with the hydrogels

ALP is a marker enzyme for early-maturity osteoblasts. The ALP staining (Fig. 3A) and quantitative analysis (Fig. 3B) of rBMSCs were performed after 7 days of culture. The results show that there was no significant difference in ALP activity between Induced group and GelMA group. The ALP activity of rBMSCs was significantly enhanced in ad-MVFs/GelMA group compared to the other groups (Fig. 3A). The quantitative results were consistent with the ALP staining (Fig. 3B). ARS was conducted to assess the mineral ability of rBMSCs. More calcium nodules were observed in the ad-MVFs/GelMA group than that in the other groups after 21 days of induction (Fig. 3C). In addition, the results of quantitative analysis also indicate that the ad-MVFs/GelMA group could produce a large amount of calcium deposition, exhibiting obvious osteogenic activity. The results of qPCR show that the ad-MVFs/GelMA hydrogels could promote the expression of osteogenesis-related genes, such as alkaline phosphatase (*Alpl*), runt-related transcription factor 2 (*Runx2*), collagen type I alpha 1 chain (*Col1a1*), secreted

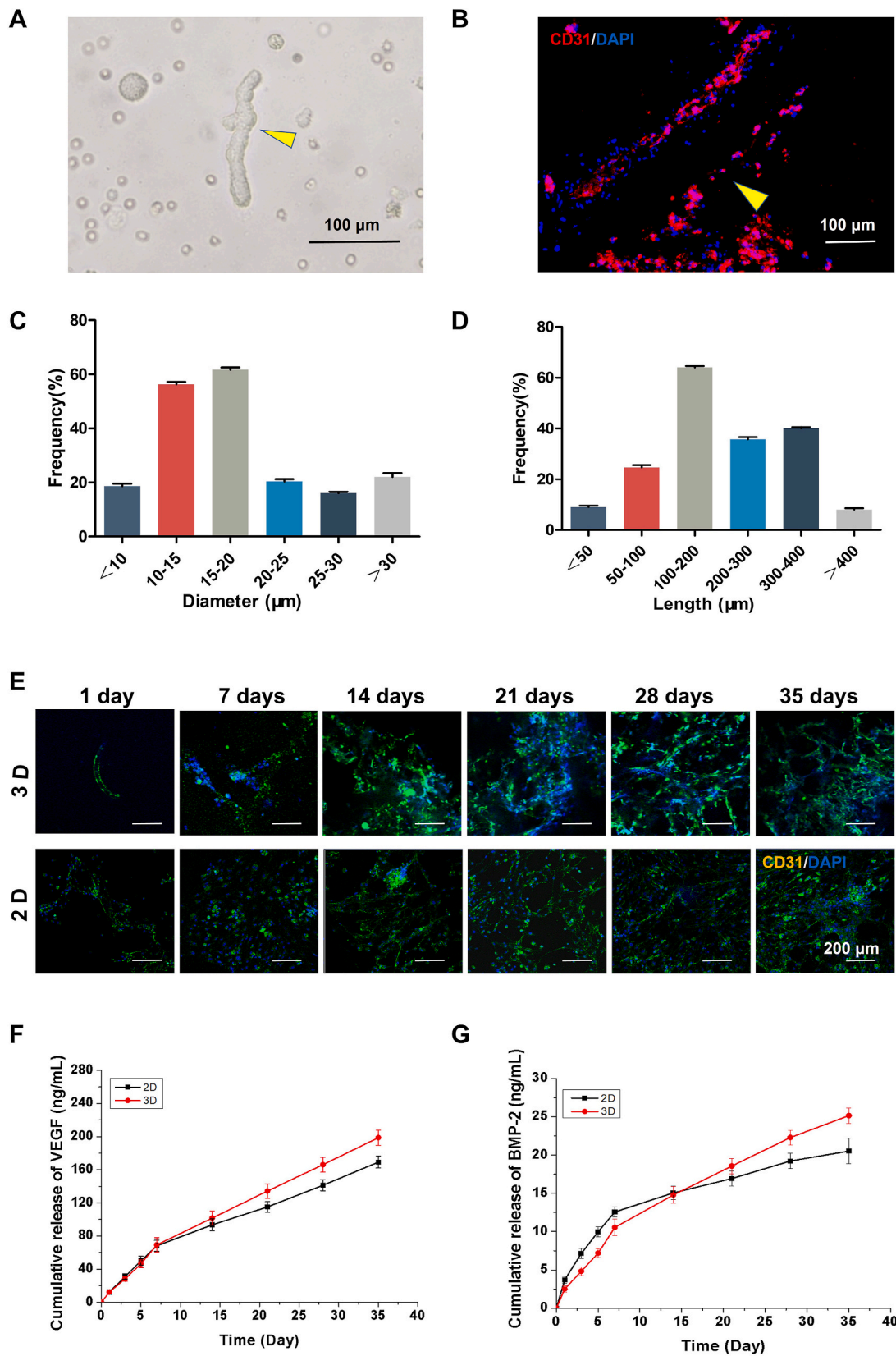


Figure 1. Characterizations of ad-MVFs. (A) The morphology of freshly isolated ad-MVFs under light microscopy. (B) ad-MVFs were stained by CD31 (red) and DAPI (blue). The yellow arrow indicates ad-MVF. The diameter (C) and length (D) of freshly isolated ad-MVFs. (E) Immunofluorescence images of ad-MVFs cultured at 2D and 3D conditions at different time points. Green indicates CD31 and blue indicates DAPI. The concentration of VEGF (F) and BMP-2 (G) in the medium of ad-MVFs cultured at 2D or 3D conditions (n = 3).

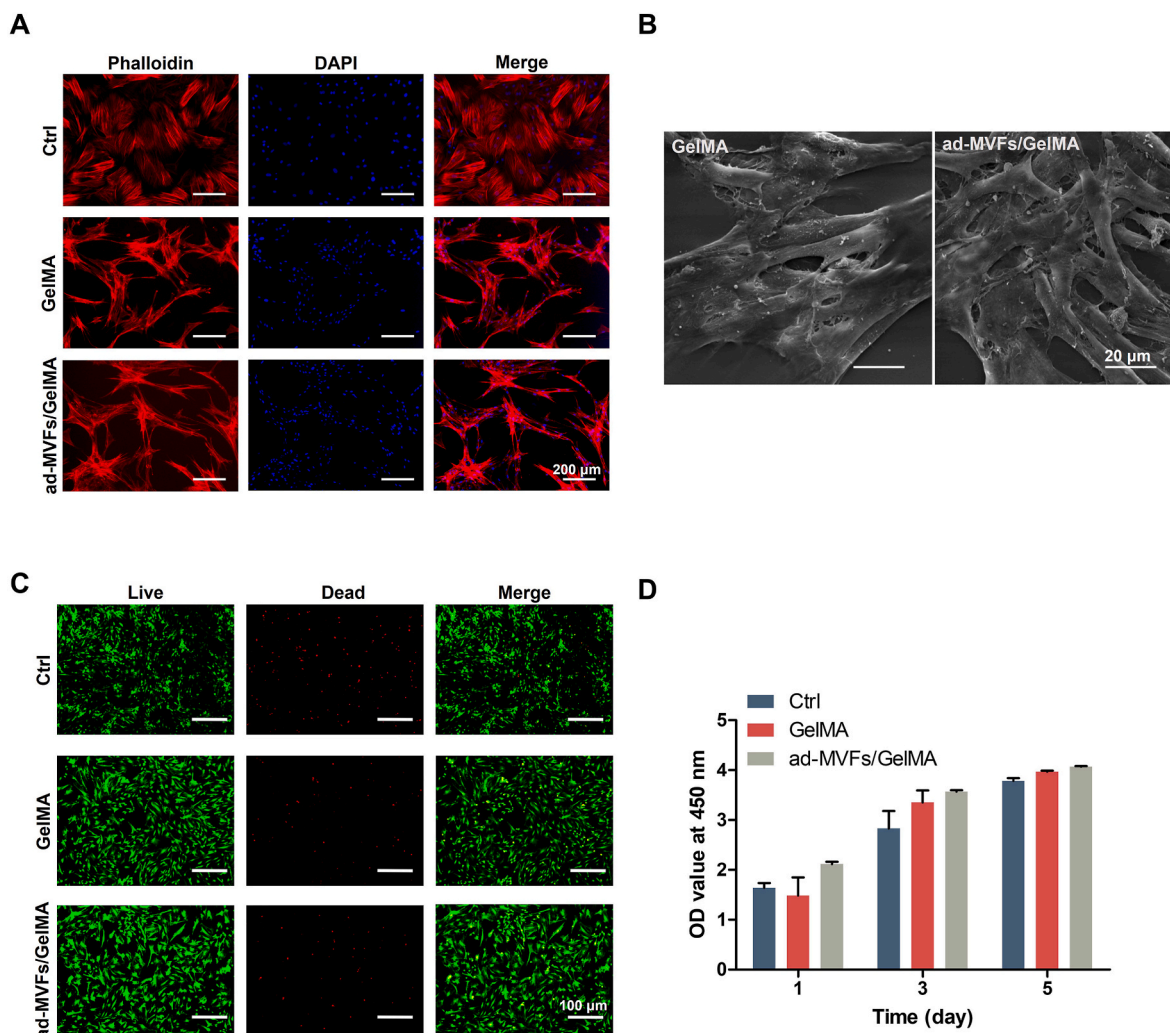


Figure 2. Growth of rBMSCs on the hydrogels. (A) The images of cytoskeleton staining. (B) SEM images of rBMSCs on the surface of GelMA and ad-MVFs/GelMA hydrogels. (C) The images of live/dead staining. (D) Cell proliferation measurement by CCK-8 assay.

phosphoprotein 1 (*Spp1*), and bone gamma-carboxyglutamate protein (*Bglap*) (Fig. 4). The results of Western blot indicate that the protein expression including that the expression of RUNX2, OPN, COL1, and OCN was significantly increased in ad-MVFs/GelMA group compared to others, which was consistent with the results of qPCR (Fig. 4). All the above demonstrate that ad-MVFs/GelMA hydrogels showed excellent osteoinductive activity.

3.7. *In vitro* osteoclastogenesis of cells cultured with hydrogels

Cells within the RANKL + group displayed heightened osteoclast characteristics in comparison to the RANKL-group, which did not undergo osteoclast induction. Notably, there were no discernible differences observed in the quantity and size of osteoclast-positive cells among the RANKL+, GelMA, and ad-MVFs/GelMA groups (Fig. S4, Supporting Information).

3.8. Bone formation ability of the hydrogels in rat skull defects

The efficacy of hydrogels in facilitating bone formation was evaluated by implanting them into skull defects in rats. 3D reconstruction images captured at 4 weeks post-surgery revealed minimal new bone formation in the Ctrl group, a modest amount in the GelMA group, and a significantly higher level in the ad-MVFs/GelMA group (Fig. 5A). Remarkably, the bone volume percentage (BV/TV) in the ad-MVFs/

GelMA group reached approximately 22 % at the 4th week, demonstrating a substantial increase compared to other groups. This trend continued, with 3D reconstruction images at 8 weeks showcasing enhanced new bone formation in the ad-MVFs/GelMA group, and a notable BV/TV value of approximately 41.7 %, which is significantly higher than the other groups.

Corroborating the micro-CT results, histological analyses through H&E (Fig. 5C) and Masson (Fig. 5D) staining underscored the superior bone formation ability of the ad-MVFs/GelMA group at both 4 and 8 weeks in comparison to the control and GelMA groups. Additionally, CD31 immunofluorescence at 4 and 8 weeks post-implantation demonstrated the presence of new blood vessels across all groups, with a discernibly higher vascular density in the ad-MVFs/GelMA group (Fig. 5E). Impressively, by the 8th week, the ad-MVFs/GelMA group exhibited the formation of a well-defined vascular network, showcasing exceptional potential for vascularization (Fig. 5E and F). This finding is consistent with the results obtained from *in vitro* tubule experiments (Fig. S5, Supporting Information).

4. Discussion

Vascularization is a fundamental requirement for bone repair. Developing predictable and sufficient vascular networks in scaffolds remains one of the major challenges for bone tissue engineering [35]. Various strategies for *in vitro* vascularization of the bone tissue scaffolds

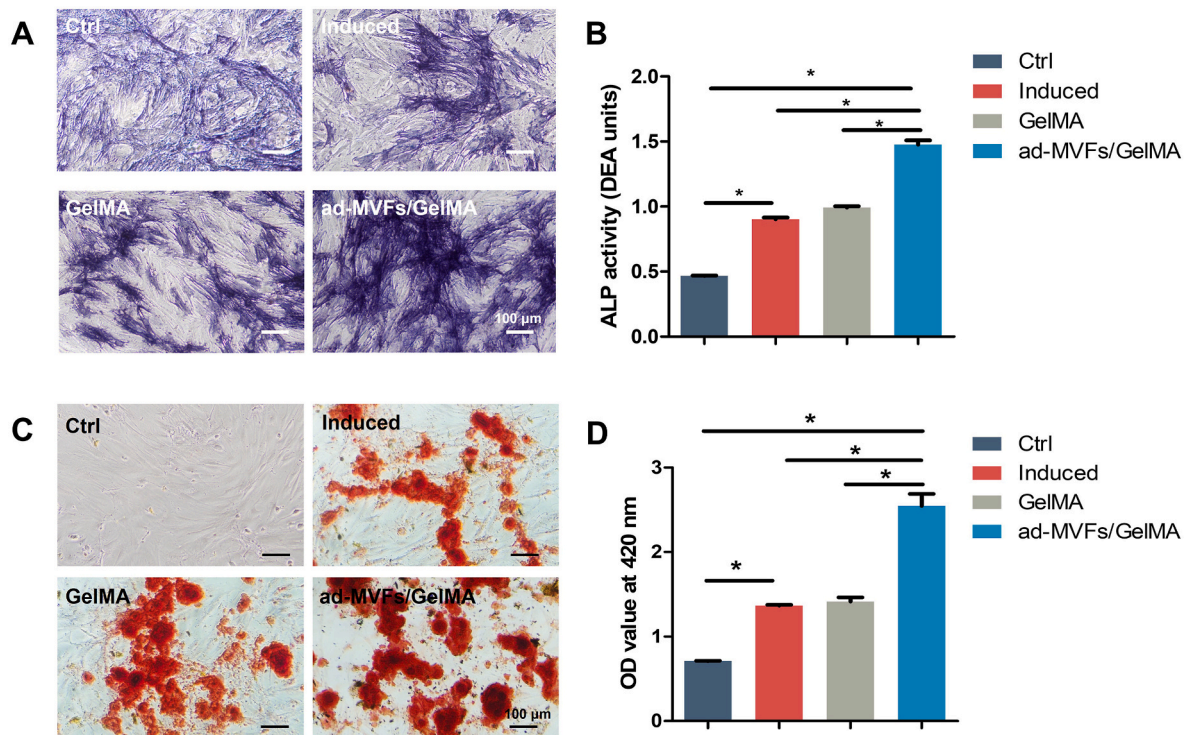


Figure 3. *In vitro* osteogenic differentiation of rBMSCs cultured with hydrogels. (A) ALP staining of the rBMSCs after osteogenic induction for 7 days, and (B) Quantitative analysis of ALP activity. (C) ARS of rBMSCs after osteogenic induction for 21 days, and (D) Quantitative analysis of ARS. *, $p < 0.05$ ($n = 5$).

have been developed and implemented in the past [36–39]. Recently, the strategies for vascularization are based on the use of angiogenic growth factors, the implantation of endothelial cells, microfabrication of blood vessels through bioprinting, and microsurgical principles [40,41]. Each strategy has its specific advantages and disadvantages. Various studies demonstrate that added exogenous VEGF to bone scaffolds could significantly promote new blood vessel formation and bone regeneration [42]. However, some growth factors show a short half-life and optimizing drug release remains a challenge [43]. It has been reported that endothelial cells can adhere and differentiate in endothelialized biomimetic microvessels, promoting bone repair by vascularization [3]. Through 3D printing technology, highly ordered tissue engineering scaffolds can be manufactured, simulating the internal environment and providing physical and chemical support for cell regulation and survival [44]. It has been reported that bio-ink which contains both HUVECs and human bone marrow mesenchymal stem cells (hBMSCs) was used in pre-vascularization 3D-printed polycaprolactone (PCL) scaffolds, and achieving excellent osteogenesis after implanting the scaffolds into critical size femoral defects of rats [45]. However, both strategies mentioned above exhibited limited survival rate of implanted cells. Microsurgical techniques can achieve the purpose of vascularization by anastomosing the blood vessels carried by the graft with the host blood vessels. However, this approach is technically challenging and requires a high level of skill on the part of the operator. Another drawback is the need for two major surgeries, and a treatment period of several months. Not only that, all these methods could not make the scaffold vascularized quickly enough after implantation. Thus, it is necessary to explore a more effective way to accelerate revascularization.

ad-MVFs emerge as a promising candidate for vascularization, leveraging the inherent microvessels within adipose tissues. These fragments exhibit exceptional vascularization potential, providing a faster and more efficient means to reconstruct vascular tissues from these minute tissue fragments. ad-MVFs, derived from adipose tissue in a brief timeframe, present with intact arterial, capillary, or venous morphology, and boast a rich composition of diverse pluripotent stem

cells and macrophages [35]. These cells reside within the vessel walls of microvascular segments or, at the very least, tightly attach to perivascular locations [5]. This advantageous localization ensures that transplanted stem cells remain within their physiological stem cell ecological niche, thereby promoting survival, self-renewal, proliferation, mobilization, and differentiation [36]. In comparison to stem cells derived from a single adipose tissue, those associated with microvascular fragments showcase heightened proliferation rates and increased gene expression related to neural, osteogenic, and adipose differentiation [5]. Flow cytometry analysis highlights the presence of cells in the microvascular debris expressing the surface marker (Sca)-1/vascular endothelial growth factor receptor-2 (VEGFR-2), a key identifier for endothelial progenitor cells [37]. Endothelial progenitor cells play a dual role by not only producing angiogenic growth factors but also demonstrating the ability to develop into new vascular structures *in vitro* and *in vivo*, a critical factor contributing to the high angiogenic potential of microvascular fragments [38]. Freshly isolated microvascular fragments further include macrophages, reported to play a pivotal role in promoting the reorganization of ad-MVFs into a novel microvascular network and expediting its maturation. Moreover, macrophages exhibit immunomodulatory functions and release an array of proinflammatory and pro-fibrotic cytokines [39]. These released cytokines attract diverse immune cells to the biomaterial implantation site, participating in the regulation of collagen deposition and binding of the implant to the surrounding host tissue [40]. Consequently, ad-MVFs, with their intact vascular morphology, demonstrate a superior vascular differentiation potential compared to single endothelial scaffolds. This underscores the intriguing prospect of harnessing waste adipose tissues for this purpose.

Cultivating ad-MVFs in isolation for extended periods poses significant challenges due to their small size and inherent susceptibility to disintegration. Recognizing the advantageous role of the physiological 3D environment in fostering the angiogenic process, GelMA emerged as an ideal carrier to ensure the stability of ad-MVF vascular morphology. The decision to employ GelMA is rooted in its ability to provide a supportive milieu for sustained ad-MVF culture. Notably, the intricacies of

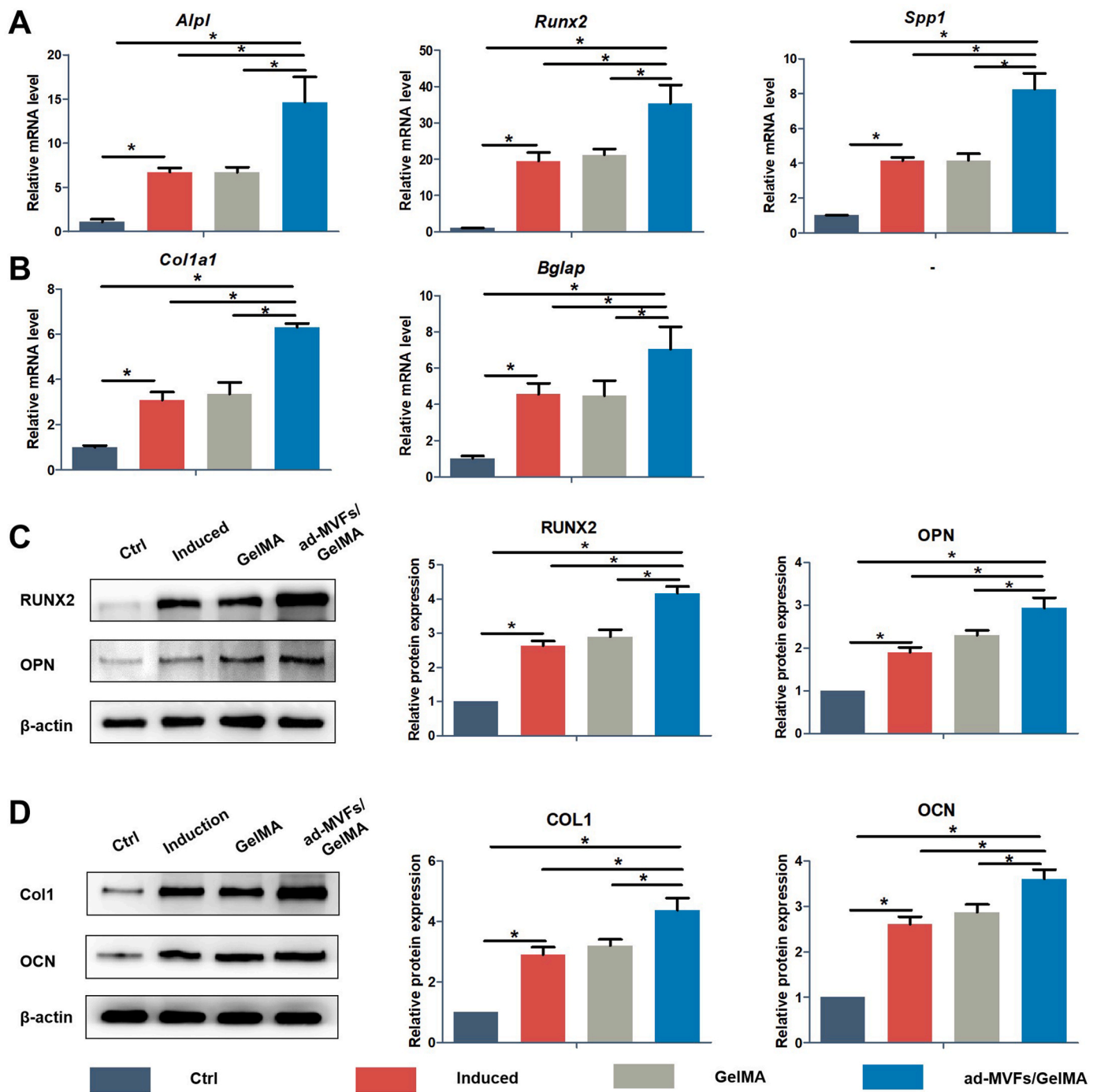


Figure 4. Expression of osteogenesis-related genes and proteins in rBMSCs during *in vitro* osteogenic induction. The gene expression of *Alpl*, *Runx2* and *Spp1* after osteogenic induction for 7 days (A), and *Col1a1* and *Bglap* on day 14 (B). (C) Western blot images of the RUNX2 and OPN proteins and the quantitative analysis of these proteins after osteogenic induction for 7 days. (D) Protein expression of COL1 and OCN and the quantitative analysis of these proteins after osteogenic induction for 14 days. *, $p < 0.05$ (n = 5).

cell-to-cell contact within a 3D culture setting better emulate the physiological conditions of native tissue compared to conventional 2D culture methods. Prior studies have underscored the efficacy of 3D culture in enhancing cell survival, promoting superior cell proliferation, and fostering differentiation [35]. In the current investigation, the utilization of GelMA hydrogel for ad-MVF culture revealed its efficacy in preserving the original vascular morphology. By the 7th day of culture, ad-MVFs exhibited notable growth, generating new branches from the extremities of the original vascular structures. These newly sprouted branches interconnected, reshaping into a discernible vascular network.

In stark contrast, ad-MVFs cultured under 2D conditions experienced a gradual disintegration, leading to the loss of the initial vascular morphology. In this scenario, the fragments dispersed into cells that colonized the bottom of the culture plate (Fig. 1C). This comparative analysis underscores the pivotal role of GelMA in maintaining the structural integrity of ad-MVFs and highlights the superiority of 3D culture in preserving the physiological features essential for successful vascularization.

To elucidate the role of ad-MVFs in bone repair, we assessed the content of crucial cytokines, VEGF and BMP-2, by collecting culture

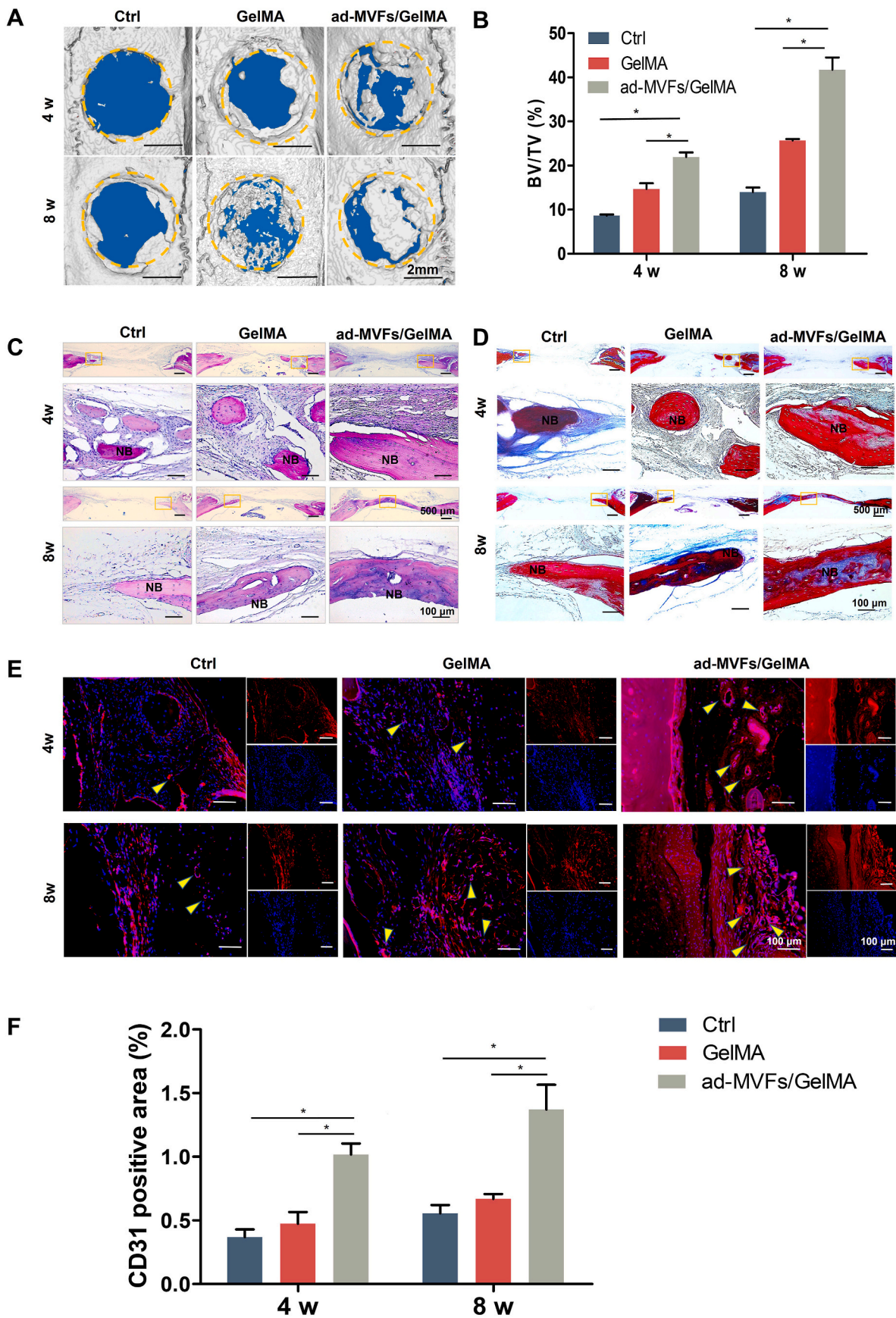


Figure 5. The repair of rat calvarial critical-sized defects by the ad-MVFs/GelMA hydrogels at 4 and 8 weeks after implantation, respectively. (A) Reconstructed micro-CT images and (B) Quantitative analysis of bone volume/tissue volume (BV/TV). Representative images of (C) H&E staining, (D) Masson staining and (E) Immunofluorescence (CD31). (F) Quantitative analysis of CD31 expression positive areas *, $p < 0.05$ ($n = 3$). (NB indicates new bone, yellow arrows indicate vessels)

medium from ad-MVFs cultivated under both 3D and 2D conditions. VEGF and BMP-2 have garnered recognition as potent cytokines pivotal for angiogenesis and osteogenesis. Taking VEGF as an exemplar, its significance in angiogenesis and bone formation is underscored by its multifaceted impact, including the promotion of endothelial cell survival, proliferation, migration, and differentiation [46]. Additionally, VEGF regulates vessel wall permeability and plays a crucial role in epithelialization and collagen deposition during bone repair [47]. Moreover, VEGF mediates the survival and differentiation of chondrocytes and osteoblasts, alongside contributing to osteoclast recruitment [48]. BMP-2, extensively employed in tissue regeneration, enhances the recruitment of osteoblast progenitor cells and facilitates osteogenic differentiation of stem cells [49]. Signaling through the Smad and MAPK pathways, BMP-2 activates transcription factors RUNX2 and OSX, instigating osteoblast-specific gene expression for accelerated bone formation [50]. The reported synergy between VEGF and BMP-2 in regulating cell communication during angiogenesis and osteogenesis emphasizes the importance of their coordinated delivery [51]. Furthermore, upregulation of BMP-2 expression in response to VEGF and low oxygen levels in bone defects enhances the therapeutic potential [52]. Our investigation suggests that the ad-MVFs/GelMA hydrogel exerts its bone repair influence through the release of these growth factors. Significantly, the quantification of VEGF and BMP-2 from ad-MVFs in 3D culture conditions surpassed that in 2D culture. This disparity can be attributed to the interconnected networks formed by 3D-cultured ad-MVFs, fostering superior cell proliferation and differentiation, consequently augmenting growth factor secretion. Conversely, 2D-cultured ad-MVFs experienced disintegration, settling at the dish bottom post-isolation, limiting space for prolonged proliferation. Hence, the findings underscore the superior vascular morphology maintenance and sustained growth factor secretion of ad-MVFs in 3D culture, substantiating their role in promoting vascularization and bone regeneration.

5. Conclusion

In this study, ad-MVFs were isolated from adipose tissue and cultured in 3D hydrogel microenvironment, exhibiting an inherent capacity for autonomous assembly and interconnection, and thereby forming vascular networks within the hydrogel. These ad-MVFs consistently release essential vascular growth factors and osteogenic factors, promoting the regeneration of blood vessels and new bone within cranial defects. Looking forward to prospective clinical applications, the discarded adipose tissue from patients emerges as a valuable reservoir of resources. The isolated ad-MVFs, with their demonstrated potential for tissue regeneration, are poised to make a substantial contribution to the personalized repair of patients' own tissues. This approach holds a distinct advantage over alternative pre-vascularization methods, as the use of one's autologous adipose tissue as a donor is not only more feasible but also safer, facilitating a more straightforward path for clinical translation and enhancing the prospects for meaningful therapeutic impact.

Data availability

The raw processed data required to reproduce these findings are available upon request.

Declaration of AI and AI-assisted technologies in the writing process

AI tools were not applied in this manuscript.

Declaration of competing interest

The authors declare that they have no known competing financial

interests or personal relationships that could have appeared to influence the work reported in this paper.

Acknowledgements

This work was supported by the National Key Research and Development Program of China (No. 2020YFC1107402), International Cooperation Project of Ningbo City (No. 2023H013), the National Natural Science Foundation of China (No. 32171350), Jiangsu Province Science and Technology Plan Special Fund (BE2022730), the Priority Academic Program Development of Jiangsu Higher Education Institutions (PAPD), and Medical and Health Science and Technology Innovation Project of Suzhou (No. SKY2022105, SKJYD2021077). Postdoctoral Fellowship Program of CPSF (BX20230253, GZB20230505), the China Postdoctoral Science Foundation, Basic cutting-edge innovation cross project of Suzhou Medical College of Soochow University (YXY2302010).

Appendix A. Supplementary data

Supplementary data to this article can be found online at <https://doi.org/10.1016/j.jot.2024.04.002>.

References

- [1] Zhang H, Zhang M, Zhai D, Qin C, Wang Y, Ma J, et al. Polyhedron-like biomaterials for innervated and vascularized bone regeneration. *Adv Mater* 2023; 35(42):2302716.
- [2] Zhuang PZ, Yao Y, Su XX, Zhao YA, Liu K, Wu XP, et al. Vascularization and neuralization of bioactive calcium magnesium phosphate/hydrogels for wound healing. *Compos Part B-Eng* 2022;242:110030.
- [3] Wang J, Wang H, Wang Y, Liu Z, Li Z, Li J, et al. Endothelialized microvessels fabricated by microfluidics facilitate osteogenic differentiation and promote bone repair. *Acta Biomater* 2022;142:85–98.
- [4] Bu S, Yu ML, Chen Q, Chen D, Xia PF, Li GF, et al. Construction of poly-(γ -benzyl-L-glutamate) composite microcarriers with osteogenic and angiogenic properties for the restoration of alveolar bone defects. *Compos Part B-Eng* 2022;242:110085.
- [5] Frazier TP, Hamel K, Wu X, Rogers E, Lassiter H, Robinson J, et al. Adipose-derived cells: building blocks of three-dimensional microphysiological systems. *Biomater Transl* 2021;2(4):301–6.
- [6] Laschke MW, Menger MD. The simpler, the better: tissue vascularization using the body's own resources. *Trends Biotechnol* 2022;40(3):281–90.
- [7] Pill K, Melke J, Muhleder S, Pultar M, Rohringer S, Priglinger E, et al. Microvascular networks from endothelial cells and mesenchymal stromal cells from adipose tissue and bone marrow: a comparison. *Front Bioeng Biotechnol* 2018;6: 156.
- [8] Wrublewsky S, Weinzierl A, Hornung I, Prates-Roma L, Menger MD, Laschke MW, et al. Co-transplantation of pancreatic islets and microvascular fragments effectively restores normoglycemia in diabetic mice. *NPJ Regen Med* 2022;7(1):67.
- [9] Kamat P, Frueh FS, McLuckie M, Sanchez-Macedo N, Wolint P, Lindenblatt N, et al. Adipose tissue and the vascularization of biomaterials: stem cells, microvascular fragments and nanofat-a review. *Cytotherapy* 2020;22(8):400–11.
- [10] Sun X, Wu J, Qiang B, Romagnuolo R, Gagliardi M, Keller G, et al. Transplanted microvessels improve pluripotent stem cell-derived cardiomyocyte engraftment and cardiac function after infarction in rats. *Sci Transl Med* 2020;12(562).
- [11] Nunes SS, Greer KA, Stiening CM, Chen HY, Kidd KR, Schwartz MA, et al. Implanted microvessels progress through distinct neovascularization phenotypes. *Microvasc Res* 2010;79(1):10–20.
- [12] Laschke MW, Kleer S, Scheuer C, Schuler S, Garcia P, Eglin D, et al. Vascularisation of porous scaffolds is improved by incorporation of adipose tissue-derived microvascular fragments. *Eur Cell Mater* 2012;24:266–77.
- [13] Horwitz EM, Le Blanc K, Dominici M, Mueller I, Slaper-Cortenbach I, Marini FC, et al. Clarification of the nomenclature for MSC: the international society for cellular therapy position statement. *Cytotherapy* 2005;7(5):393–5.
- [14] McDaniel JS, Pilia M, Ward CL, Pollot BE, Rathbone CR. Characterization and multilineage potential of cells derived from isolated microvascular fragments. *J Surg Res* 2014;192(1):214–22.
- [15] Spater T, Tobias AL, Menger MM, Nickels RM, Menger MD, Laschke MW. Biological coating with platelet-rich plasma and adipose tissue-derived microvascular fragments improves the vascularization, biocompatibility and tissue incorporation of porous polyethylene. *Acta Biomater* 2020;108:194–206.
- [16] Gruonu G, Stone AL, Schwartz MA, Hoying JB, Williams SK. Encapsulation of ePTFE in prevascularized collagen leads to peri-implant vascularization with reduced inflammation. *J Biomed Mater Res* 2010;95(3):811–8.
- [17] Shepherd BR, Hoying JB, Williams SK. Microvascular transplantation after acute myocardial infarction. *Tissue Eng* 2007;13(12):2871–9.

- [18] Salamone M, Rigogliuso S, Nicosia A, Campora S, Bruno CM, Ghersi G. 3D collagen hydrogel promotes in vitro langerhans islets vascularization through ad-MVFs angiogenic activity. *Biomedicines* 2021;9(7):739.
- [19] Frueh FS, Spater T, Korbel C, Scheuer C, Simson AC, Lindenblatt N, et al. Prevascularization of dermal substitutes with adipose tissue-derived microvascular fragments enhances early skin grafting. *Sci Rep-Uk* 2018;8(1):10977.
- [20] Spater T, Frueh FS, Menger MD, Laschke MW. Potentials and limitations of Integra (R) flowable wound matrix seeded with adipose tissue-derived microvascular fragments. *Eur Cell Mater* 2017;33:268–78.
- [21] Stone 2nd R, Rathbone CR. Microvascular fragment transplantation improves rat dorsal skin flap survival. *Prs-Glob Open* 2016;4(12):1140.
- [22] Xu X, Liang C, Gao X, Huang H, Xing X, Tang Q, et al. Adipose tissue-derived microvascular fragments as vascularization units for dental pulp regeneration. *J Endod* 2021;47(7):1092–100.
- [23] Li J, Ma J, Feng Q, Xie E, Meng Q, Shu W, et al. Building osteogenic microenvironments with a double-network composite hydrogel for bone repair. *Research* 2023;6:21.
- [24] Sivaraj KK, Adams RH. Blood vessel formation and function in bone. *Development* 2016;143(15):2706–15.
- [25] Novosel EC, Kleinhans C, Kluger PJ. Vascularization is the key challenge in tissue engineering. *Adv Drug Deliv Rev* 2011;63(4–5):300–11.
- [26] Yu H, VandeVord PJ, Mao L, Matthew HW, Wooley PH, Yang SY. Improved tissue-engineered bone regeneration by endothelial cell mediated vascularization. *Biomaterials* 2009;30(4):508–17.
- [27] Zhou F, Cui C, Sun S, Wu S, Chen S, Ma J, et al. Electrospun ZnO-loaded chitosan/PCL bilayer membranes with spatially designed structure for accelerated wound healing. *Carbohydr Polym* 2022;282:119131.
- [28] Liu J, Chuah YJ, Fu J, Zhu W, Wang DA. Co-culture of human umbilical vein endothelial cells and human bone marrow stromal cells into a micro-cavitary gelatin-methacrylate hydrogel system to enhance angiogenesis. *Mat Sci Eng C-Mater* 2019;102:906–16.
- [29] Wang Z, Tian Z, Menard F, Kim K. Comparative study of gelatin methacrylate hydrogels from different sources for biofabrication applications. *Biofabrication* 2017;9(4):044101.
- [30] Klotz BJ, Gawlitta D, Rosenberg A, Malda J, Melchels FPW. Gelatin-methacryloyl hydrogels: towards biofabrication-based tissue repair. *Trends Biotechnol* 2016;34(5):394–407.
- [31] Li J, Han F, Ma J, Wang H, Pan J, Yang G, et al. Targeting endogenous hydrogen peroxide at bone defects promotes bone repair. *Adv Funct Mater* 2021;32(10):2111208.
- [32] Zhou B, Jiang X, Zhou X, Tan W, Luo H, Lei S, et al. GelMA-based bioactive hydrogel scaffolds with multiple bone defect repair functions: therapeutic strategies and recent advances. *Biomater Res* 2023;27(1):86.
- [33] Li L, Li J, Zou Q, Zuo Y, Cai B, Li Y. Enhanced bone tissue regeneration of a biomimetic cellular scaffold with co-cultured MSCs-derived osteogenic and angiogenic cells. *Cell Prolif* 2019;52(5):12658.
- [34] Arora D, Robey PG. Recent updates on the biological basis of heterogeneity in bone marrow stromal cells/skeletal stem cells. *Biomater Transl* 2022;3(1):3–16.
- [35] Diomedea F, Marconi GD, Fonticoli L, Pizzicanella J, Merciaro I, Bramanti P, et al. Functional relationship between osteogenesis and angiogenesis in tissue regeneration. *Int J Mol Sci* 2020;21(9):3242.
- [36] Conde-Gonzalez A, Glinka M, Dutta D, Wallace R, Callanan A, Oreffo ROC, et al. Rapid fabrication and screening of tailored functional 3D biomaterials: validation in bone tissue repair - Part II. *Biomater Adv* 2023;145:213250.
- [37] Zhou X, Qian Y, Chen L, Li T, Sun X, Ma X, et al. Flowerbed-inspired biomimetic scaffold with rapid internal tissue infiltration and vascularization capacity for bone repair. *ACS Nano* 2023;17(5):5140–56.
- [38] Han X, Sun M, Chen B, Saiding Q, Zhang J, Song H, et al. Lotus seedpod-inspired internal vascularized 3D printed scaffold for bone tissue repair. *Bioact Mater* 2021;6(6):1639–52.
- [39] Cheng WX, Liu YZ, Meng XB, Zheng ZT, Li LL, Ke LQ, et al. PLGA/beta-TCP composite scaffold incorporating cucurbitacin B promotes bone regeneration by inducing angiogenesis. *J Orthop Transl* 2021;31:41–51.
- [40] Yu L, Wei Q, Li J, Wang H, Meng Q, Xie E, et al. Engineered periosteum-diaphysis substitutes with biomimetic structure and composition promote the repair of large segmental bone defects. *Compos Part B-Eng* 2023;252:110505.
- [41] Guo S, He C. Bioprinted scaffold remodels the neuromodulatory microenvironment for enhancing bone regeneration. *Adv Funct Mater* 2023;33(40):2304172.
- [42] Zhang S, Chen J, Yu Y, Dai K, Wang J, Liu C. Accelerated bone regenerative efficiency by regulating sequential release of BMP-2 and VEGF and synergism with sulfated chitosan. *ACS Biomater Sci Eng* 2019;5(4):1944–55.
- [43] Ren Y, Kong W, Liu Y, Yang X, Xu X, Qiang L, et al. Photocurable 3D-printed PMBG/TCP scaffold coordinated with PTH (1-34) bidirectionally regulates bone homeostasis to accelerate bone regeneration. *Adv Healthcare Mater* 2023;12(25):2300292.
- [44] Zhang Y, He F, Zhang Q, Lu H, Yan S, Shi X. 3D-printed flat-bone-mimetic bioceramic scaffolds for cranial restoration. *Research* 2023;6:255.
- [45] Nulty J, Freeman FE, Browe DC, Burdis R, Ahern DP, Pitacco P, et al. 3D bioprinting of prevascularised implants for the repair of critically-sized bone defects. *Acta Biomater* 2021;126:154–69.
- [46] Kang F, Yi Q, Gu P, Dong Y, Zhang Z, Zhang L, et al. Controlled growth factor delivery system with osteogenic-angiogenic coupling effect for bone regeneration. *J Orthop Transl* 2021;31:110–25.
- [47] Dreyer CH, Kjaergaard K, Ding M, Qin L. Vascular endothelial growth factor for in vivo bone formation: a systematic review. *J Orthop Transl* 2020;24:46–57.
- [48] Qin C, Zhang H, Chen L, Zhang M, Ma J, Zhuang H, et al. Cell-laden scaffolds for vascular-innervated bone regeneration. *Adv Healthcare Mater* 2023;12(13):2201923.
- [49] Lv Z, Hu T, Bian Y, Wang G, Wu Z, Li H, et al. A MgFe-LDH nanosheet-incorporated smart thermo-responsive hydrogel with controllable growth factor releasing capability for bone regeneration. *Adv Mater* 2023;35(5):2206545.
- [50] Wang LL, Chen L, Wang JP, Wang LY, Gao CY, Li B, et al. Bioactive gelatin cryogels with BMP-2 biomimetic peptide and VEGF: a potential scaffold for synergistically induced osteogenesis. *Chin Chem Lett* 2022;33(4):1956–62.
- [51] Dastimoghadam E, Fahimipour F, Tongas N, Tayebi L. Microfluidic fabrication of microcarriers with sequential delivery of VEGF and BMP-2 for bone regeneration. *Sci Rep-Uk* 2020;10(1):11764.
- [52] Talavera-Adame D, Wu G, He Y, Ng TT, Gupta A, Kurtovic S, et al. Endothelial cells in co-culture enhance embryonic stem cell differentiation to pancreatic progenitors and insulin-producing cells through BMP signaling. *Stem Cell Rev Rep* 2011;7(3):532–43.